agriculture

MDPI

Article

Exploration of Piezo Channels in Bread Wheat (*Triticum aestivum* L.)

Amandeep Kaur [1], Madhu [1], Alok Sharma [1], Kashmir Singh [2] and Santosh Kumar Upadhyay [1,*]

[1] Department of Botany, Panjab University, Chandigarh 160014, India
[2] Department of Biotechnology, Panjab University, Chandigarh 160014, India
* Correspondence: skupadhyay@pu.ac.in; Tel.: +91-172-2534001; Fax: +91-172-2779510

Abstract: Piezo channels belong to an important class of cell membrane-bound, Ca^{2+}-permeable, mechanosensitive channels consisting of a pore and multiple transmembrane helices. In plants, the functional aspects of Piezo channels have been less studied than other mechanosensitive channels. However, a few studies that have been carried out indicate the involvement of Piezo channels in stress response and developmental processes. In our analysis, we identified a total of three *Piezo* genes in the *Triticum aestivum* genome. The phylogenetic analysis revealed the monocot and dicot-specific clustering of Piezo proteins. The gene and protein structure analysis indicated their conserved architecture. The promoter region of each of the three *Piezo* genes contained light-, growth-and development-, hormone-, and stress-responsive *cis*-regulatory elements. Moreover, the differential expression of *Piezo* genes in tissue developmental stages and under abiotic and biotic stress conditions indicated their probable role in plant growth and development and various stresses. The quantitative real-time polymerase chain reaction (qRT-PCR) analysis suggested that *TaPiezo1-D* might be involved in Ca^{2+} homeostasis. In addition, protein–protein interaction indicated their precise role in glucose, hormone and stress responses. The miRNA interaction analysis further suggested their participation in signaling cascades and biological processes. The present study will extend our understanding about Piezo channels in Ca^{2+} mediated signaling in plants under various stresses and provide a path for the functional validation of *TaPiezo* genes in future research.

Keywords: abiotic; biotic; hormone; miRNA; stress

Citation: Kaur, A.; Madhu; Sharma, A.; Singh, K.; Upadhyay, S.K. Exploration of Piezo Channels in Bread Wheat (*Triticum aestivum* L.). *Agriculture* **2023**, *13*, 783. https://doi.org/10.3390/agriculture13040783

Academic Editor: Mark O. Winfield

Received: 11 February 2023
Revised: 22 March 2023
Accepted: 27 March 2023
Published: 29 March 2023

1. Introduction

Plants sense various mechanical stimuli, including touch, sound, gravity, osmotic pressure etc., throughout their life cycle. These mechanical stimuli cause plasma membrane deformation, leading to the activation of various channels, which allow the ion permeation and downstream signaling cascade [1]. These channels are known as stretch-activated channels or mechanosensitive (MS) channels. Five types of MS channels have been identified: mechanosensitive channel of small conductance-like (MscS-like or MSL); mid1-complementing activity (MCA); two-pore potassium channel (TPK); hyperosmolality-induced [Ca^{2+}] increase (OSCA) and Piezo channels in plants [2]. In contrast to the MSL, MCA, TPK and OSCA, the Piezo channels are relatively less explored.

Piezo channels are primarily known for their contribution in various aspects of animal mechanosensation [3–5]. Initially, Piezo1 and Piezo2 were discovered in mouse (*Mus musculus*) as Ca^{2+}-permeable ion channels [6]. Moreover, Piezo proteins were reported as regulator of membrane potential and Ca^{2+} signaling [5–8]. The structural studies of Piezo1 by high-resolution cryo-electron microscopy revealed its three-bladed propeller shape, consisting of an arched transmembrane region and ion-conducting central pore [9–11]. The homologous proteins of Piezo have been reported in fungi, animals and plants [6]. In the majority of plants, one to three *Piezo* genes have been reported [12]. Most of the species of algae, bryophytes and pteridophytes comprised only one *Piezo* gene. However,

Ostreococcus lucimarinus, *Physcomitrella patens* and *Sphagnum fallax*, each harbor two *Piezo* genes [12,13]. Monocot species, for instance, *Brachypodium distachyon*, *Brachypodium stacei*, *Oryza sativa Japonica*, *Sorghum bicolor*, *Setaria italica*, *Setaria viridis*, *Zea mays* etc., consisted of only one *Piezo* gene [12,13]. In the case of dicot species, one *Piezo* gene was found in each of *Arabidopsis thaliana*, *Nicotiana attenuate*, *Solanum species* etc., two genes in each of *Medicago truncatula*, *Vigna radiata*, *Vitis vinifera*, *Eucalyptus grandis*, *Ricinus communis*, *Brassica rapa* etc., and three genes in *Glycine max* and *Gossypium raimondii* [12,13].

In *A. thaliana*, the mutant *AtPiezo* showed abnormal root growth on agar medium, which indicated their involvement in normal root growth. Additionally, AtPiezo channel facilitates the influx of Ca^{2+} ions in the root cap upon mechanical stimuli, and therefore, it acts as a mechanosensory protein [12,14]. Furthermore, *AtPiezo* mutants show enhanced susceptibility to viral infection, which revealed the role of *AtPiezo* in biotic stress responses [15]. In *P. patens*, the vacuolar morphology is reported to controlled by PpPiezo1 and PpPiezo2 by facilitating the Ca^{2+} efflux from the vacuole in response to hypo-osmotic stress [16]. In *O. sativa*, the *Piezo* gene exhibited significant expression in roots, leaves, pistils, lemmas and ovaries [13]. Moreover, the occurrence of gibberellin-, abscisic acid (ABA)- and jasmonic acid-related *cis*-regulatory elements in the *Piezo* gene of *O. sativa* suggested its participation in stress-related signal transduction [13].

To date, no Piezo channel has been identified in major food crop, i.e., *T. aestivum*. In the current study, we identified three *Piezo* genes in the genome of *T. aestivum*. Furthermore, using in silico approaches, various analyses such as that of chromosomal localization, phylogenetic, gene structure, *cis*-regulatory elements, and protein structure have been carried out. To elucidate the functioning of *Piezo* genes, their expression patterns were analyzed in three developmental stages of five tissues and heat, drought, salt and fungal stresses using the available high-throughput RNA sequence data. To validate the functioning of Piezo protein in Ca^{2+} homeostasis, the quantitative real-time polymerase chain reaction (qRT-PCR) of one *Piezo* gene homeolog, i.e., *TaPiezo1-D*, was performed. Protein–protein and miRNA interaction analyses were also carried out. Collectively, this study will create a path for the functional validation of TaPiezo proteins in the future.

2. Materials and Methods

2.1. Identification of TaPiezos and Their Chromosomal Distribution

Firstly, the bidirectional BLAST hit approach was used to find the Piezo proteins of *T. aestivum*. The protein model sequences were retrieved from the IWGSC (IWGSC RefSeq assembly v2.0, accessed on 13 June 2022) and Ensembl Plant databases. The known protein sequences of Piezo channel of *A. thaliana* and *O. sativa* were used as queries in the BLASTp search as opposed to the above-retrieved protein sequences of *T. aestivum*. The occurrence of a functionally conserved domain in all TaPiezo proteins was confirmed using the Conserved Domain Database search and SMART server [17,18].

The sub-genomic and chromosomal information of *TaPiezo* genes was retrieved from the Ensembl Plant database. Furthermore, the chromosomal maps were prepared through MapInspect (mapinspect.software.in-former.com/, accessed on 14 January 2023). The homeologous clustering of identified *Piezo* was based on $\geq$90% sequence similarity [19–21]. The *Piezo* of *T. aestivum* were named according to the recommended guidelines of gene symbolization (http://wheat.pw.usda.gov/ggpages/wgc/98/Intro.htm, accessed on 17 July 2022).

2.2. Phylogenetic Analysis

The full-length protein sequences of Piezo channels from eight plants, namely, *A. thaliana*, *B. rapa*, *B. distachyon*, *G. max*, *N. attenuate*, *O. sativa*, *S. bicolor*, and *Z. mays*, along with *T. aestivum*, were used for the phylogenetic analysis. Firstly, the Muscle algorithm program was used for the alignment of protein sequences. Then, the phylogenetic tree was created using the protein sequence alignment on MEGA X software [22]. The neighbor-joining method was employed with 1000 bootstrap replicates.

2.3. Gene Structure Analysis

To construct the gene structure, the coding sequence (CDS) and genomic sequence of each *TaPiezo* gene were aligned using the GSDS 2.0 server [23]. The gene structure was demonstrated in the form of exon–intron patterning and intron phase distribution.

2.4. Cis-Regulatory Element Analysis

The *cis*-regulatory elements were predicted among the 1.5 kb upstream promoter of each *TaPiezo* gene using the PlantCARE database [24].

2.5. Physicochemical, Motif Analyses and Multiple Sequence Alignment

The physicochemical characterizations of Piezo proteins including length, isoelectric point (pI), molecular weight (MW) and grand average of hydropathicity (GRAVY) value were carried out using the online Expasy tool [25]. The number of transmembrane helices, the signal peptide and the subcellular localization of each Piezo protein were examined through the TMHMM-2.0 (https://services.healthtech.dtu.dk/service.php?TMHMM-2.0, accessed on 19 July 2022), SignalP 5.0. (https://services.healthtech.dtu.dk/service.php?SignalP-5.0, accessed on 19 July 2022) and Cello server [26], respectively. Moreover, the 15 conserved motifs were predicted through MEME (Multiple Expectation Maximization for Motif Elicitation) suite version 5.1.1 server at default parameters, which were further scanned through the scan motif server [27] (https://myhits.sib.swiss/cgi-bin/motif_scan, accessed on 21 July 2022). Furthermore, to analyze the conserved residues, the multiple sequence alignment of Piezo proteins was carried out using the ClustalW in Bioedit [28]. The 3-dimensional (3D) structure of TaPiezo1-A was predicted using the Pyre2 (http://www.sbg.bio.ic.ac.uk/phyre2/html/page.cgi?id=index, accessed on 13 January 2023) and illustrated by the Pymol (https://pymol.org/2/, accessed on 15 January 2023).

2.6. Expression Profiling of Piezo Genes

To decipher the putative functioning of *Piezo* genes, the expression profiling of these genes was performed under several tissue developmental stages and stress treatments. An openly accessible URGI database (https://urgi.versailles.inra.fr/files/RNASeqWheat, accessed on 26 July 2022) was used to retrieve high-throughput RNA sequence data.

To investigate the expression profiling of *TaPiezo* in tissue developmental stages, the high-throughput RNA sequence data, derived from the root, leaf, stem, spike, and grain tissues generated in two biological replicates, were used [29,30]. The developmental stages were: z10, z13, z39 for roots; z30, z32, z65 for stem; z10, z23, z71 for leaf; z32, z39 z65 for spike; and z71, z75, z85 for grain. The expression values were calculated in the form of fragments per kilobase of transcripts per million mapped (FPKM) reads through Trinity packages. Furthermore, the Expression ATLAS was used for the confirmation of expression data [31,32].

The effect of abiotic stresses on *TaPiezo* was studied by performing the expression profiling with the usage of high-throughput RNA sequence data produced in duplicates after 1 and 6 h of heat stress (HS) (40 °C), drought stress (DS) (20% Poly Ethylene Glycol (PEG) and combined heat and drought stress (HD) from leaf tissue [33]. During salt stress, 6, 12, 24 and 48 h of salt-treated (150 mM NaCl) root tissue was used for the production of RNA sequence data [34].

Moreover, the effect of. *Blumeria graminis* (Bgt) and *Puccinia striiformis* (Pst) were studied by performing expression profiling. The high-throughput RNA sequence data was extracted after 24, 48 and 72 h of fungal infestation in triplicate [35]. The expression readings were computed into FPKM reads through the Trinity package [31]. Furthermore, the heat maps were made through the Hierarchical Clustering Explorer (HCE) 3.5 software and hierarchical clustering was performed with the Euclidean distance method [36].

2.7. qRT-PCR Analysis

Firstly, sodium hypochlorite (1.2%) along with 10% ethanol were used for surface sterilization of *T. aestivum* (cv. Chinese spring) seeds. After washing with double autoclaved water, the seeds were kept at 4 °C for stratification. The next day, seeds were allowed to germinate at room temperature. Thereafter, the germinated seedlings were placed in a plant growth chamber at 16 h of light and 8 h of the dark period, 60% relative humidity and 22 °C temperature. After 7 days, the $CaCl_2$ (20 mM) treatment was given to the seedlings with Murashige and Skoog media. Subsequently, the samples were collected in liquid nitrogen after 6, 12, 24 and 48 h of stress treatment. The total RNA from root tissues was isolated using Spectrum TM Plant Total RNA kit (Sigma, Saint Louis, MI, USA). For the production of contamination free RNA, the isolated samples were treated using the TURBO DNA-free™ Kit (Invitrogen, Carlsbad, CA, USA). The quality of isolated RNA samples were examined via agarose gel electrophoresis, and quantity via Nanodrop spectrophotometer. Subsequently, the cDNAs were prepared with the Superscript III First-Strand Synthesis Super-mix (Invitrogen, Carlsbad, CA, USA) from one microgram of RNA. The qRT-PCR experiment was carried out at CFX96 Real-Time PCR (BioRad, Hercules, CA, USA) using SYBR Green, cDNA and gene-specific primers, following recommended procedures [37]. Moreover, for the internal control, an ADP-ribosylation factor of *T. aestivum* (*TaARF1*) was utilized during the experiment (Table 1). The delta-delta CT ($2^{-\Delta\Delta CT}$) method was employed to compute the expression values, and the experiment was practiced in three biological replicates (n = 3), which were displayed as mean standard deviation (SD) [38,39].

Table 1. List of qRT-PCR primers.

Gene Name	5′-3′
*TaARF*_Forward primer	TGATAGGGAACGTGTTGTTGAGGC
*TaARF*_Reverse primer	AGCCAGTCAAGACCCTCGTACAAC
*TaPiezo1-D*_Forward primer	AGGAGAGGATTTCACAATTGGAGGCTG
*TaPiezo1-D*_Reverse primer	CTTCAACCAAAGAAAGGACAGCAGCAG

2.8. Protein–Protein and miRNA-Interaction Analysis

The protein–protein interactions of TaPiezo proteins were predicted through the STRING server (http://stringdb.org, accessed on 27 July 2022) accessed on 27 July 2022) [40]. The psRNATarget database (http://plantgrn.Noble.org/psRNATarget/, accessed on 28 July 2022) was explored to find the interacting miRNAs of *TaPiezo* genes [41]. Furthermore, the interaction networks have been prepared using the Cytoscape tool (https://cytoscape.org/download.html, accessed on 14 November 2022).

3. Results

3.1. Identification and Chromosomal Localization of TaPiezo

A total of three *TaPiezo* genes (*TraesCS3A02G192500.1*, *TraesCS3B02G222000.1* and *TraesCS3D02G196400.1*) were identified in the *T. aestivum* genome through a BLASTp search of Piezo sequences of *A. thaliana* (*AT2G48060*) and *O. sativa* (*Os01g0388500*). These three genes shared ≥90% sequence similarity with and were derived from A, B and D sub-genome and were therefore considered homoeologous genes. The genes *TraesCS3A02G192500.1*, *TraesCS3B02G222000.1* and *TraesCS3D02G196400.1* were named as *TaPiezo1-A*, *TaPiezo1-B* and *TaPiezo1-D*, respectively. The chromosomal positions of *TaPiezo1-A*, *TaPiezo1-B* and *TaPiezo1-D* were on the short arm of chromosome 3A, 3B and 3D, respectively (Figure 1; Table S1). All the *TaPiezo* genes were found on the forward strand of their respective chromosomes.

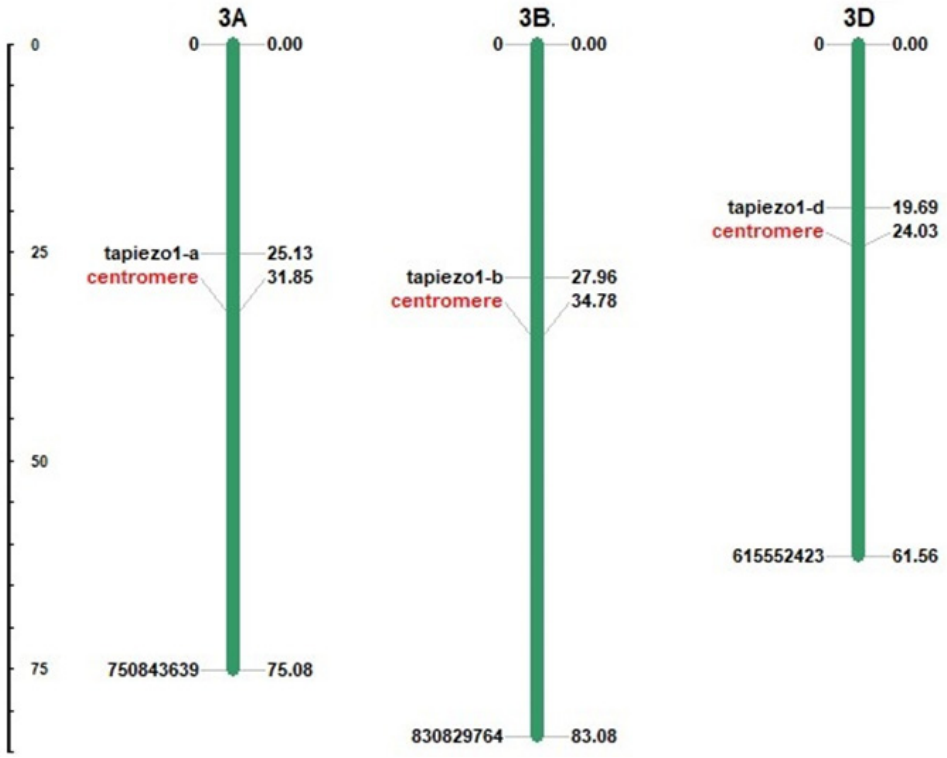

Figure 1. The chromosomal position of *TaPiezo* genes. *TaPiezo* genes are found on chromosomes 3A, 3B and 3D of *T. aestivum*.

3.2. Phylogenetic Analysis

To study the evolutionary relationships, the phylogenetic tree was constructed with full-length Piezo protein sequences of *A. thaliana*, *G. max*, *B. rapa*, *B. distachyon*, *N. attenuate*, *O. sativa*, *T. aestivum*, *S. bicolor* and *Z. mays* (Figure 2). The phylogenetic tree showed the clustering of Piezos into two groups: I and II. Piezo proteins of dicot species were clustered in group I, while Piezo proteins of monocots were clustered in group II. Moreover, the Piezo proteins of *T. aestivum* were closely clustered in the phylogenetic tree (Figure 2).

3.3. Gene Structure Analysis

The gene structure analysis was carried out to investigate the length of CDS, the number of introns and exons, their organization, and intron phase distribution. The predicted length of CDS for each *TaPiezo1-A* and *TaPiezo1-D* was 7494 base pair (bp), while *TaPiezo1-B* was 7492 bp. Each of the *TaPiezo* genes showed the presence of 21 exons and 20 introns. The patterns of exons and introns were found to be similar among all *Piezo* genes of *T. aestivum* (Figure 3; Table S1). The majority of the introns (42%) of *TaPiezo* genes were found in intron phase 1, followed by phase 0 (35%) and phase 2 (23%) (Figure 3).

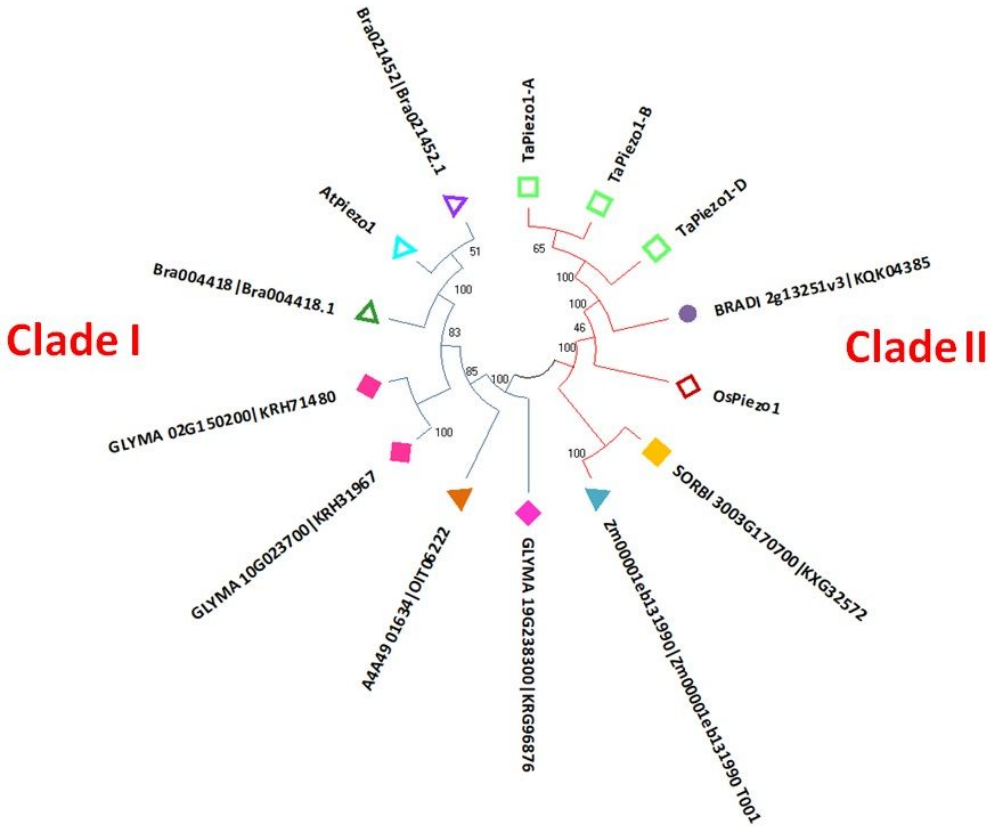

Figure 2. Phylogenetic analysis of Piezo proteins of *A. thaliana* (AtPiezo1), *O. sativa* (OsPiezo1), *T. aestivum* (TaPiezo1-A, TaPiezo1-B and TaPiezo1-D), *B. rapa* (Bra004418|Bra004418.1, Bra021452|Bra021452.1), *B. distachyon* (BRADI_2g13251v3|KQK04385), *G. max* (GLYMA_19G238300|KRG96876, GLYMA_10G023700|KRH31967, GLYMA_02G150200|KRH71480), *N. attenuate* (A4A49_01634|OIT06222), *S. bicolor* (SORBI_3003G170700|KXG32572), and *Z. mays* (Zm00001eb131990|Zm00001eb131990_T001). The phylogenetic tree represents the clustering of Piezo proteins into two clades, and each clade is colored differently.

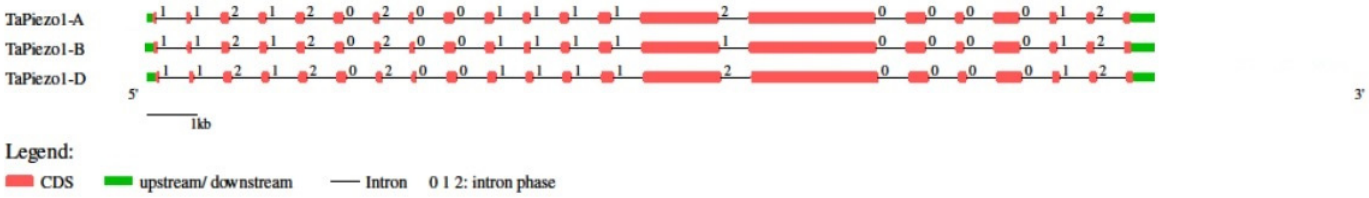

Figure 3. Gene structure analysis of *TaPiezo* genes. The figure represents the exon–intron organization and intron phase distribution in each *TaPiezo* gene, generated by the GSDS 2.0.

3.4. Cis-Regulatory Element Analysis

The analysis of *cis*-regulatory elements is a significant approach for studying the involvement of Piezo channels in a diverse range of biological processes. In the current analysis, we have identified a wide range of *cis*-regulatory elements that were light, growth and development, stress and hormone responsive (Table 2). The predicted light-responsive *cis*-regulatory elements were G-Box, Sp1, G-box, TCCC-motif, AE-box, ACE, TCT-motif, I-box and Box 4. The *cis*-regulatory elements which showed their connection with various plant growth and developmental processes were O2-site (zein metabolism regulation), RY-element (seed-specific regulation), CAT-box (meristem expression), GCN4_motif (endosperm development), CCGTCC-box (meristem specific activation), etc. (Table 2). Several identified stress-related *cis*-regulatory elements were LTR (low-temperature responsive), GC-motif (anoxic specific inducibility), ARE (anaerobic induction), W-box (responsive to

pathogenic attack), MBS (involved in drought inducibility), TC-rich repeats (defense and stress-responsive), DRE (dehydration responsive element), MYB, MYC (drought-responsive elements), WRE3 (wound responsive), etc. In addition to these, the most common hormone-responsive *cis*-regulatory elements found in the *Piezo* genes were ABRE, ABRE4, ABRE3a, AT~ABRE (Abscisic acid-responsive), TGA-element (Auxin responsive), P-box (gibberellin responsive), CGTCA-motif and TGACG-motif (methyl jasmonate responsive), and TCA-element (salicylic acid-responsive) (see Table 2).

Table 2. Various types of *Cis*-regulatory elements of *TaPiezo* genes.

Gene Name	Light Response	Growth and Development	Stress Response	Hormone Response
TaPiezo1-A	G-box, TCT-motif, I-box, TCCC-motif, G-Box, Box 4	CCGTCC-box, GCN4_motif, CCGTCC motif, AAGAA-motif	ARE, as-1, LTR, STRE, WRE3, A-box, W box, MYB, GC-motif, Myb-binding site, MYB-like sequence, TC-rich repeats	TCA-element, ABRE, CGTCA-motif, TGA-element, TGACG-motif
TaPiezo1-B	AE-box, G-box, G-Box,	O2-site, RY-element, CCGTCC-box, CCGTCC motif	MYC, Myb-binding site, STRE, MYB recognition site, MYB, WRE3, LTR, ARE, Myb, as-1, A-box	TGACG-motif, ABRE, CGTCA-motif
TaPiezo1-D	Sp1, G-box, TCT-motif, ACE	CCGTCC motif, O2-site, CCGTCC-box, CAT-box	W box, LTR, MYB-like sequence, WRE3, GC-motif, TC-rich repeats, MYC, A-box, box S, Myb, MBS, STRE, as-1, Myb-binding site, DRE core, MYB recognition site, MYB	CGTCA-motif, AT~ABRE, ABRE4, TGACG-motif, TATC-box, P-box, ABRE3a, ABRE

3.5. Protein Characterization

The length of each TaPiezo1-A and TaPiezo1-D protein was 2497 amino acid (aa) residues, while the length of TaPiezo1-B protein was 2496 aa residues. The calculated MW of TaPiezo1-A and TaPiezo1-D was 286.7 kilodaltons (kDa) (Table S1), while the MW of TaPiezo1-B was 286.4 kDa. The isoelectric points calculated for TaPiezo1-A, TaPiezo1-B and TaPiezo1-D were 8.17, 8.24 and 8.21, respectively (Table S1). The GRAVY values for TaPiezo1-A, TaPiezo1-B and TaPiezo1-D were 0.229, 0.230 and 0.226, respectively. The sub-cellular localization analysis predicted the plasma membrane localization of TaPiezo channels. In addition, no signal peptide was found in the TaPiezo proteins (Table S1).

Domains are considered the structural and functional units of proteins, and therefore, it is important to study the domain composition of a protein. In the current study, domain analysis at Pfam and SMART server suggested the occurrence of a very conserved domain, known as the Piezo R-Ras-binding domain (PF12166) in all the identified Piezo proteins of *T. aestivum* (Figure 4A; Table S2). This conserved domain comprised 392 aa residues in each TaPiezo protein. Additionally, the TaPiezo1-A and TaPiezo1-B consisted of 31 transmembrane helices, while TaPiezo1-D consisted of 33 transmembrane helices (Figure 4A).

A total of 15 motifs have been predicted in Piezo proteins of *T. aestivum* (Figure 4B). All the motifs were predominately found in each TaPiezo protein and revealed their conserved nature. Motifs 2, 6 and 14 were identified as part of the conserved Piezo R-Ras-binding domain, and motifs 7 and 9 were identified as part of transmembrane helices. Furthermore, casein kinase II phosphorylation and protein kinase C phosphorylation sites were also found in the majority of the motifs of TaPiezo proteins. However, cAMP- and cGMP-dependent protein kinase phosphorylation, ASN-glycosylation, tyrosine kinase phosphorylation and N-myristoylation sites were detected in motifs 8, 9 and 13, and, 5 and 13, and, 3, 9, 11 and 14, respectively.

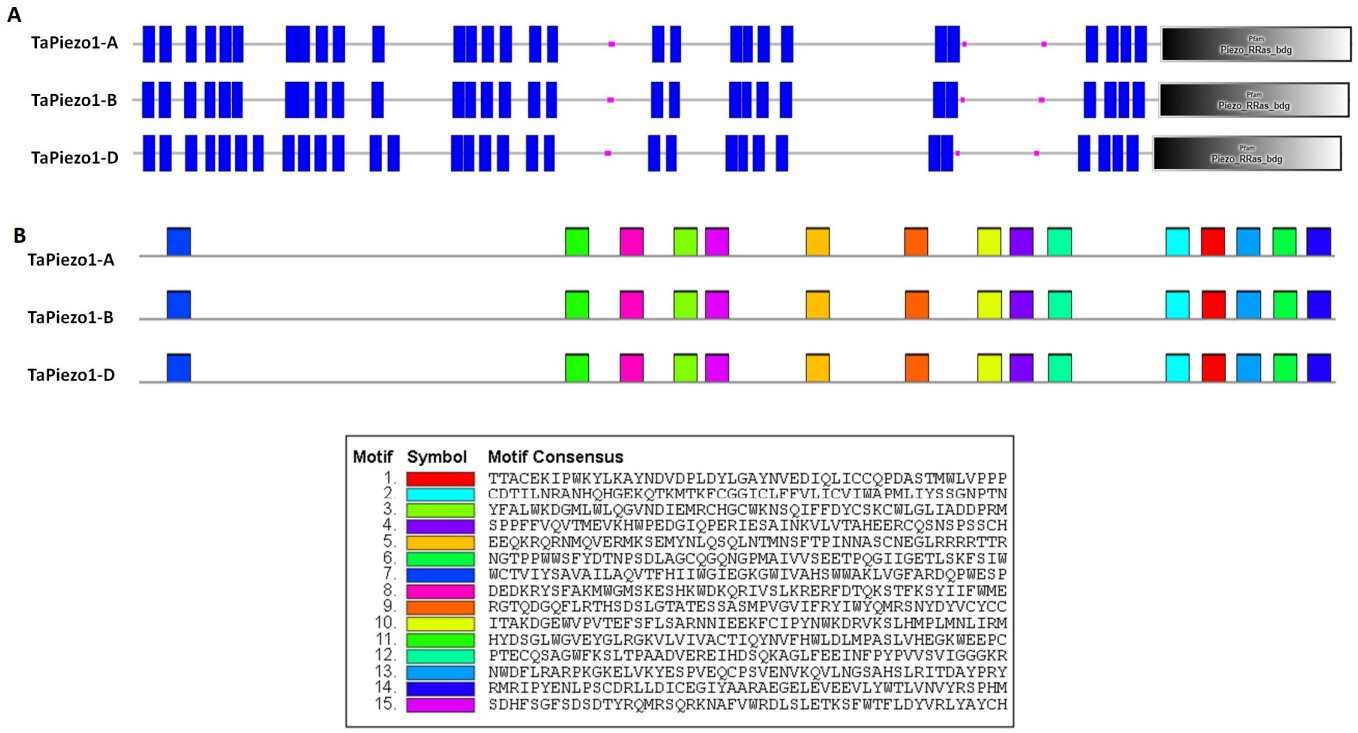

Figure 4. Protein structure analysis of TaPiezo proteins. (**A**) represents the schematic diagram of TaPiezo proteins obtained from the SMART server. (**B**) represents the arrangement of 15 conserved motifs of each TaPiezo protein, represented as colored boxes.

Furthermore, the Piezo protein sequences of *A. thaliana*, *T. aestivum*, *O. sativa* and *M. musculus* were aligned using the ClustalW to highlight the conversed residues (Figure S1). All the Piezo proteins consisted of a beam domain, outer helix (OH), central cap domain (CED), inner helix (IN) and C-terminal domain (CTD) (Figure S1). Moreover, it was analyzed that OH, CED, IN and CTD were evolutionarily more conserved as compared to the beam domain in all the species. All the domains were also highlighted in the 3D structure of the TaPiezo1-A protein (Figure 5).

3.6. Expression Profiling of Piezo Genes in Tissue Developmental Stages

To study the probable functioning of *TaPiezo* genes in plant growth and development, their expression profiling was carried out in three developmental stages of the root, stem, leaf, spike and grain tissues using the high-throughput RNA sequence data [29,30]. Furthermore, the reliability of expression was confirmed by correlation analysis. The Pearson correlation value was 0.95 for various tissue developmental stages and 0.99 for stress conditions (Figure 6A,B). *TaPiezo1-A* exhibited low expression values during the various tissue development stages, except spike tissues (Figure 6C). On the other hand, *TaPiezo1-D* showed comparatively elevated expression during multiple tissue development stages including stem, leaf, root, spike and grain tissues, while *TaPiezo1-B* showed expression in stem, leaf and spike tissues. All the *TaPiezo* genes showed significant upregulation in the spike developmental stages. Overall analysis indicated that *TaPiezo* genes expressed in several tissue developmental stages, however, lacked tissue specificity.

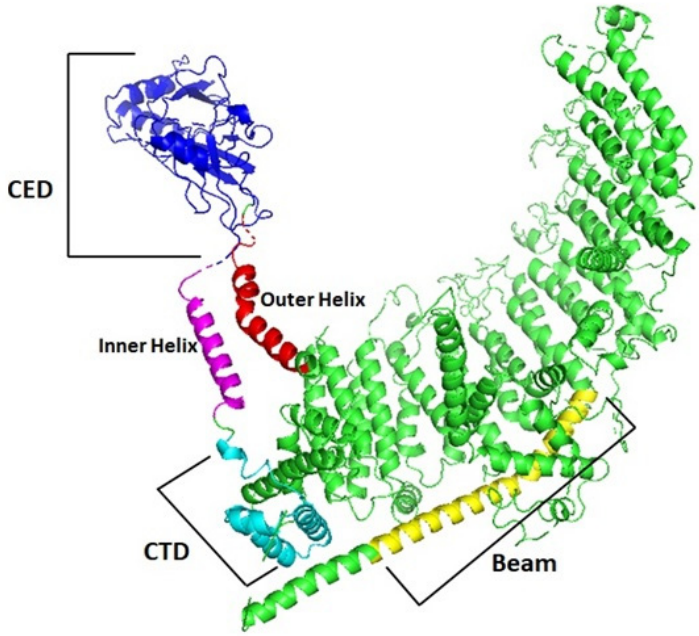

Figure 5. The three-dimensional structure of TaPiezo1-A protein. The figure displays the predicted 3D structure of TaPiezo1-A protein. The beam domain, outer helix (OH), central cap domain (CED), inner helix (IN) and C-terminal domain (CTD) are highlighted in the figure with different colors.

3.7. Expression Profiling of Piezo Genes in Abiotic and Biotic Stresses

To analyze the effect of abiotic stresses on *TaPiezo* genes, their expression values are retrieved from leaf tissues under HS, DS and HD, and from root tissues under salt stress using the respective high-throughput RNA sequence data as described in Materials and Methods [33,34]. All the genes showed significant upregulation at one hour of HS and HD. *TaPiezo1-A* showed a 5.9- and 9.2-fold higher expression at one hour of HS and HD stress as compared to control, respectively (Figure 6D). However, *TaPiezo1-B* exhibited a 4.6- and 5.9-fold upregulated expression at one hour of HS and HD, respectively. The gene *TaPiezo1-D* was 3.5- and 5.2-fold upregulated at the one hour of HS and HD stress, respectively. Moreover, *TaPiezo1-A* and *TaPiezo1-D* also showed upregulation to some extent at six hours of HS and HD treatments (Figure 6D).

During salt stress, the gene *TaPiezo1-A* showed upregulation (two-fold) at six hours of stress, and downregulation at 12, 24 and 48 h (Figure 6E). The gene *TaPiezo1-D* was found to be downregulated at 6, 12, 24 and 48 h, while *TaPiezo1-B* at 48 h of salt stress (Figure 6E).

To study the effect of biotic stresses on *TaPiezos*, their expression values were retrieved from leaf tissues under the stress of two fungal pathogens, i.e., Bgt and Pst using the high-throughput RNA sequence data [35]. The gene *TaPiezo1-A* was upregulated (two-fold) at 72 h of Bgt infestation (Figure 6F). The gene *TaPiezo1-B* exhibited significant upregulation, i.e., 3-, 3.2- and 6.5-fold at 24, 48 and 72 h of Bgt infestation and 4-fold at 48 h of Pst infestation, respectively. The gene *TaPiezo1-D* showed 1.7- and 3.2-fold upregulation after 48 and 72 h of Bgt infestation, and 1.6- and 1.3-fold after 48 and 72 h of Pst infestation, respectively (Figure 6F).

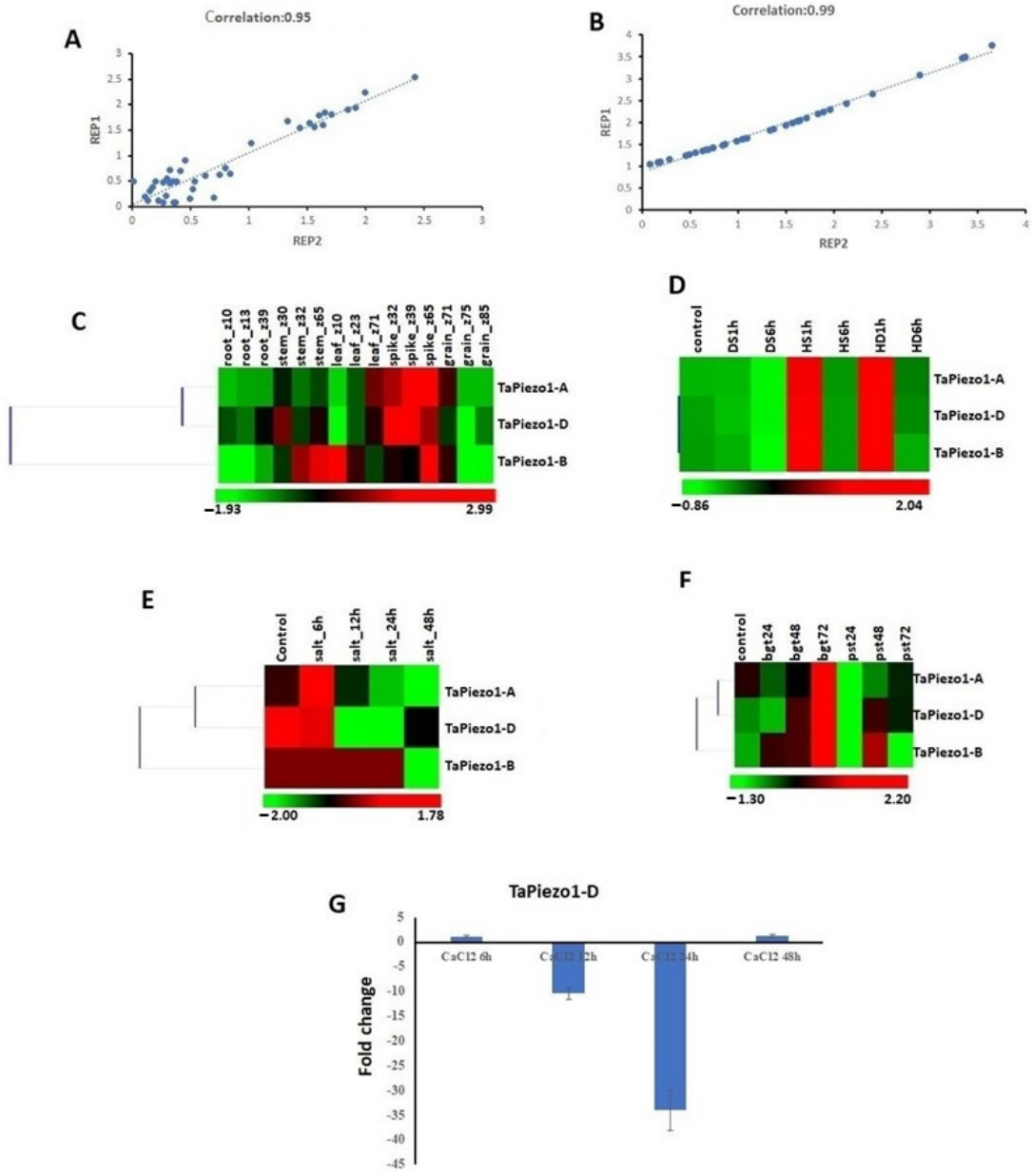

Figure 6. Correlation, expression and qRT-PCR analysis. Figure shows correlation analyses between replicates of expression data in (**A**) tissue developmental stages and (**B**) stress conditions. Heat map (**C**) shows the clustering and expression profiling *TaPiezo* genes in tissue developmental stages. The Heat maps (**D**–**F**) show the expression profile of *TaPiezo* genes under (**D**) drought stress, heat stress, and heat–drought stress, (**E**) salt stress and (**F**) during the treatment of *Blumeria graminis* (Bgt) and *Puccinia striiformis* (Pst), respectively. The low and high expressions are represented by green and red colors, respectively, in the color bar. Graph (**G**) shows the qRT-PCR results of *TaPiezo1-D* under $CaCl_2$ stress at 6, 12, 24, and 48 h of treatments. The bar graphs indicate the fold change in *TaPiezo1-D* gene expression under treatments as compared to the control condition.

3.8. qRT-PCR Analysis

The qRT-PCR analysis was carried out to study the effect of $CaCl_2$ on the *Piezo* genes of *T. aestivum* in the root tissues and its role in Ca^{2+} homeostasis and signaling. One of the homeologous gene, *TaPiezo1-D*, was chosen for the qRT-PCR analysis because all the identified genes showed very high similarity. *TaPiezo1-D* gene expression was almost unaffected at six hours, while it was significantly downregulated at 12 and 24 h of $CaCl_2$ treatment (Figure 6G). At 48 h, its expression was restored.

3.9. Protein–Protein Interaction

To explore the coordinated functions of TaPiezo proteins in developmental processes, plant metabolism, and stress responses, the protein–protein interaction analysis was performed using the STRING server. The results indicated the interaction of TaPiezo1-A, TaPiezo1-B and TaPiezo1-D with seven proteins, including RNA-dependent RNA polymerase 1 (RDR1), Dolichyl-diphosphooligosacchar—e–protein glycosyltransferase subunit STT3A and STT3B, putative E3 ubiquitin-protein ligase XBAT31, Gamma-soluble NSF attachment protein (GSNAP), Protein pleiotropic regulatory locus 1 (PLR1), and Ribulose-1,5-bisphosphate carboxylase/oxygenase large subunit (RBCL) (Figure 7A).

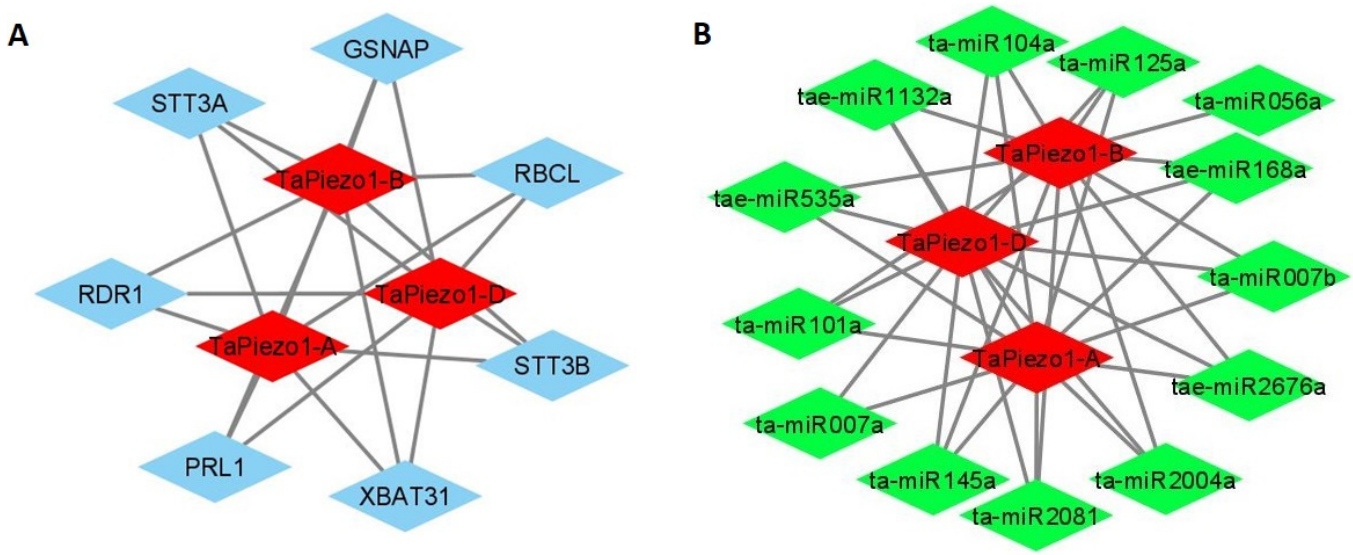

Figure 7. Protein–protein and miRNA interaction analysis of Piezo of *T. aestivum*. The network (**A**) shows the protein–protein interactions, where TaPiezo proteins are represented with red and predicted interacting proteins with blue. The interaction network (**B**) of predicted miRNA with *TaPiezo* genes. The interaction networks were built using the Cytoscape tool.

3.10. miRNAs Interaction Analysis

A total of 13 known miRNAs of *T. aestivum* showed interaction with *TaPiezo* genes. Among them, 11 miRNAs (tae-miR2676a, ta-miR125a, ta-miR2004a, tae-miR1132a, tae-miR535a, ta-miR007b, ta-miR056a, ta-miR101a, ta-miR104a, ta-miR145a and ta-miR2081) showed interaction with their targeted transcripts through cleavage mechanism (Figure 7B; Table S3). However, two miRNAs (ta-miR007a and tae-miR168a) showed translation inhibition as their mode of action. The majority of miRNAs interacted with all the *Piezo* genes of *T. aestivum*. However, the ta-miR007a interacted with *TaPiezo1-A* and *TaPiezo1-D*, and ta-miR056a interacted with only *TaPiezo1-B* gene (Figure 7B).

4. Discussion

In our study, the identification and characterization of TaPiezo channels have been performed to explore their structural features and roles in *T. aestivum*. After an extensive BLAST search, three *TaPiezo* genes were identified in the allohexaploid genome of *T. aestivum*, which were comparatively greater as compared to diploid plants such as *O. sativa*, *A. thaliana* and *Z. mays*, etc., due to its higher ploidy level [12,13]. In addition, previously, the relationship between a higher number of *Piezo* genes and ploidy composition was observed in tetraploid plant species such as *G. max* and *G. hirsutum* [12,13].

During evolutionary analysis, the clustering of Piezo proteins of monocots and dicots in separate groups of phylogenetic tree pointed towards the divergence among them. As reported in previous studies, the monocots possess only single *Piezo* and dicots possess variable number of *Piezo* genes [12,13].

The length of CDS, the number of exons and introns of the *Piezo* genes of *T. aestivum* were found comparable with the *Piezo* of *A. thaliana* [12]. The presence of a similar pattern of exons and introns among the *Piezos* of *T. aestivum* and intron distribution revealed their conserved architecture..

Furthermore, the existence of numerous *cis*-regulatory elements in the promoter of *TaPiezo* pointed towards their diverse functionality. They were predicted to be involved in stress (abiotic and biotic), hormone, light-related signaling, and plant growth and developmental processes. Previous research also indicated the presence of light, methyl jasmonate, ABA, and meristem specific *cis*-regulatory elements in the promoter of *Piezo* of *O. sativa* [13]. Several studies reported the elevation of Ca^{2+} ions in response to stress response and developmental processes [42–45]. Therefore, we have speculated that *TaPiezo* genes could facilitate the influx of Ca^{2+} ions, which further triggers the downstream signaling cascade.

The length of TaPiezo proteins and the number of transmembrane helices were comparable with Piezo proteins studied in various animals and plants [12,13,46]. The predicted subcellular localization of TaPiezo was plasma membrane, similarly to previous studies [13,46,47]. The presence of transmembrane helices further confirmed the plasma membranous localization of the TaPiezo proteins. In the current analysis, we have found the conserved beam, OH, CAP, IH and CTD, and similar findings were reported in earlier studies [10,12,13,48]. The OH, CAP, IH and CTD were the core-forming structure of Piezo proteins and were found to be highly conserved in animals as well as plants [10]. In contrast to them, the beam domain facilitates the transmission of mechanical signals to the CTD of Piezo proteins [10]. The less the beam domain was conserved suggested that there might be diversity between the signal transmission in Piezo proteins of different species.

The significant expression of all the *TaPiezo* genes in the spike indicated their probable contribution in reproductive development. *TaPiezo1-A* might be specifically involved in spike development due to its higher expression in this tissue only. However, the higher expression of *TaPiezo1-B* and *TaPiezo1-D* in numerous tissues suggested their involvement in both vegetative and reproductive tissue development. An earlier study demonstrated the GUS activity of *AtPiezo* gene in the root, leaf petioles, flower petals, silique, stalks, guard tissues, vascular tissues and pollen tissues [12,15]. Moreover, the *AtPiezo* was reported to be expressed in the columella and cap cells of the root tip, where it showed mechanical activity through Ca^{2+} elevation at the time of root growth [14]. The *Piezo* of *O. sativa* was reported to be significantly expressed in vegetative (root and leaf) and reproductive organs (pistil, ovary and lemmas) [13].

The modulated expression of *TaPiezo* genes at different hours of HS, DS, HD, salt, Bgt and Pst stresses suggested their putative functioning in defense, which was also supported by the presence of various stress-related *cis*-regulatory elements. An earlier report also demonstrated a precise role of *AtPiezo* in the suppression of systemic infection of the Cucumber and Turnip mosaic virus [15]. The altered expression of *TaPiezo1-D* gene under $CaCl_2$ stress suggested that it might be associated with Ca^{2+} homeostasis and signaling.

The interaction of TaPiezos with other proteins and miRNAs suggested their involvement in several biological processes as well as stress-responsive signaling pathways. For instance, the involvement of RDR1 in plant defense and resistance against viruses and fungus suggested that the TaPiezo proteins might be an important player in biotic stress responses [49–52]. The interaction of TaPiezo proteins with the STT3a subunit suggested their roles in adaptive responses to salt/osmotic stress [53,54]. Another identified interacting protein, PRL1, was reported as the global regulator of sugar, stress and hormone responses [55–57], thus revealing the diverse functionality of TaPiezo proteins. Moreover, the interaction of TaPiezo proteins with RBCL indicated their linkage with carbon dioxide fixation during photosynthesis. The involvement of interacting miRNAs in blast disease resistance and controlling the plant height, panicle architecture and grain shape [58,59] pointed toward the precise role of TaPiezo in plant immunity as well as growth. The induced expression of miRNA168a under ABA and other abiotic stresses suggested the

probable involvement of TaPiezos in plant stress responses [60]. The miRNA168a was reported to be responsive to a fungal pathogen *Phytophthora infestans* in *Solanum lycopersicum* [61,62]. Furthermore, the involvement of miRNA1132 in fruit development revealed the probable functioning of *TaPiezo* in reproductive development [63].

In conclusion, an inclusive analysis of the Piezo gene family in *T. aestivum* indicated their plausible participation from development to defense. The presence of *cis*-regulatory elements of *TaPiezo* genes revealed their probable functioning in a wide range of physiological processes. The expression profiling of *TaPiezo* genes indicated their role in plant developmental processes and stress responses. Their interaction with other proteins and miRNAs associated with defense responses further suggested their participation in stress response. Hence, the present analysis will facilitate a way to further explore the functions and their validation in future studies.

Supplementary Materials: The following supporting information can be downloaded at: https://www.mdpi.com/article/10.3390/agriculture13040783/s1, Table S1. Characterization of Piezo genes and proteins in *T. aestivum*; Table S2. Domain analysis of Piezo proteins of *T. aestivum*; Table S3. The predicted interacting miRNAs of TaPiezo proteins. Figure S1. Multiple sequence alignment of Piezo protein of *A. thaliana*, *M. musculus*, *O. sativa* and *T. aestivum*.

Author Contributions: S.K.U. conceived the idea and designed the experiments. A.K., M. and A.S. accomplished the whole experiments. Data analysis was performed by S.K.U., K.S. and A.K., A.K. and S.K.U. wrote the manuscript. All authors have read and agreed to the published version of the manuscript.

Funding: This research has been accomplished without external funding.

Institutional Review Board Statement: Not applicable.

Informed Consent Statement: Not applicable.

Data Availability Statement: Not applicable.

Acknowledgments: We are thankful to the Panjab University, Chandigarh, India, for providing us the research facilities, and Science and Engineering Board (SERB), Government of India (CRG/2021/000040), CSIR and UGC for the Core Research Grant and fellowships, respectively.

Conflicts of Interest: The authors declare no conflict of interest.

References

1. Hamilton, E.S.; Schlegel, A.M.; Haswell, E.S. United in diversity: Mechanosensitive ion channels in plants. *Annu. Rev. Plant Biol.* **2015**, *66*, 113–137. [CrossRef] [PubMed]
2. Hamant, O.; Haswell, E.S. Life behind the wall: Sensing mechanical cues in plants. *BMC Biol.* **2017**, *15*, 59. [CrossRef] [PubMed]
3. Kim, S.E.; Coste, B.; Chadha, A.; Cook, B.; Patapoutian, A. The role of Drosophila Piezo in mechanical nociception. *Nature* **2012**, *483*, 209–212. [CrossRef] [PubMed]
4. Ranade, S.S.; Woo, S.H.; Dubin, A.E.; Moshourab, R.A.; Wetzel, C.; Petrus, M.; Mathur, J.; Bégay, V.; Coste, B.; Mainquist, J.; et al. Piezo2 is the major transducer of mechanical forces for touch sensation in mice. *Nature* **2014**, *516*, 121–125. [CrossRef] [PubMed]
5. Murthy, S.E.; Dubin, A.E.; Patapoutian, A. Piezos thrive under pressure: Mechanically activated ion channels in health and disease. *Nat. Rev. Mol. Cell Biol.* **2017**, *18*, 771–783. [CrossRef] [PubMed]
6. Coste, B.; Mathur, J.; Schmidt, M.; Earley, T.J.; Ranade, S.; Petrus, M.J.; Dubin, A.E.; Patapoutian, A. Piezo1 and Piezo2 are essential components of distinct mechanically activated cation channels. *Science* **2010**, *330*, 55–60. [CrossRef] [PubMed]
7. Rode, B.; Shi, J.; Endesh, N.; Drinkhill, M.J.; Webster, P.J.; Lotteau, S.J.; Bailey, M.A.; Yuldasheva, N.Y.; Ludlow, M.J.; Cubbon, R.M.; et al. Piezo1 channels sense whole body physical activity to reset cardiovascular homeostasis and enhance performance. *Nat. Commun.* **2017**, *8*, 350. [CrossRef]
8. Wu, J.; Lewis, A.H.; Grandl, J. Touch, tension, and transduction–the function and regulation of Piezo ion channels. *Trends Biochem. Sci.* **2017**, *42*, 57–71. [CrossRef]
9. Ge, J.; Li, W.; Zhao, Q.; Li, N.; Chen, M.; Zhi, P.; Li, R.; Gao, N.; Xiao, B.; Yang, M. Architecture of the mammalian mechanosensitive Piezo1 channel. *Nature* **2015**, *527*, 64–69. [CrossRef]
10. Saotome, K.; Murthy, S.E.; Kefauver, J.M.; Whitwam, T.; Patapoutian, A.; Ward, A.B. Structure of the mechanically activated ion channel Piezo1. *Nature* **2018**, *554*, 481–486. [CrossRef]
11. Zhao, Q.; Zhou, H.; Chi, S.; Wang, Y.; Wang, J.; Geng, J.; Wu, K.; Liu, W.; Zhang, T.; Dong, M.Q.; et al. Structure and mechanogating mechanism of the Piezo1 channel. *Nature* **2018**, *554*, 487–492. [CrossRef] [PubMed]

12. Fang, X.; Liu, B.; Shao, Q.; Huang, X.; Li, J.; Luan, S.; He, K. AtPiezo plays an important role in root cap mechanotransduction. *Int. J. Mol. Sci.* **2021**, *22*, 467. [CrossRef] [PubMed]
13. Heng, H.; Guoqiang, H.; Jin, S.; Fengli, Z.; Dabing, Z. Bioinformatics analysis for Piezo in rice. *Reprod. Breed.* **2021**, *1*, 108–113. [CrossRef]
14. Mousavi, S.A.; Dubin, A.E.; Zeng, W.Z.; Coombs, A.M.; Do, K.; Ghadiri, D.A.; Keenan, W.T.; Ge, C.; Zhao, Y.; Patapoutian, A. PIEZO ion channel is required for root mechanotransduction in *Arabidopsis thaliana*. *Proc. Natl. Acad. Sci. USA* **2021**, *118*, e2102188118. [CrossRef]
15. Zhang, Z.; Tong, X.; Liu, S.Y.; Chai, L.X.; Zhu, F.F.; Zhang, X.P.; Zou, J.Z.; Wang, X.B. Genetic analysis of a Piezo-like protein suppressing systemic movement of plant viruses in *Arabidopsis thaliana*. *Sci. Rep.* **2019**, *9*, 3187. [CrossRef]
16. Radin, I.; Richardson, R.A.; Weiner, E.R.; Bascom, C.S.; Bezanilla, M.; Haswell, E.S. Regulation of vacuole morphology by PIEZO channels in spreading earth moss. *BioRxiv* **2020**, 2020-08. [CrossRef]
17. Marchler-Bauer, A.; Bo, Y.; Han, L.; He, J.; Lanczycki, C.J.; Lu, S.; Chitsaz, F.; Derbyshire, M.K.; Geer, R.C.; Gonzales, N.R.; et al. CDD/SPARCLE: Functional classification of proteins via subfamily domain architectures. *Nucleic Acids Res.* **2017**, *45*, D200–D203. [CrossRef]
18. Letunic, I.; Doerks, T.; Bork, P. SMART: Recent updates, new developments and status in 2015. *Nucleic Acids Res.* **2015**, *43*, D257–D260. [CrossRef]
19. Kaur, A.; Taneja, M.; Tyagi, S.; Sharma, A.; Singh, K.; Upadhyay, S.K. Genome-wide characterization and expression analysis suggested diverse functions of the mechanosensitive channel of small conductance-like (MSL) genes in cereal crops. *Sci. Rep.* **2020**, *10*, 16583. [CrossRef]
20. Madhu; Kaur, A.; Tyagi, S.; Singh, K.; Upadhyay, S.K. Exploration of glutathione reductase for abiotic stress response in bread wheat (*Triticum aestivum* L.). *Plant Cell Rep.* **2022**, *41*, 639–654. [CrossRef]
21. Kaur, A.; Sharma, A.; Dixit, S.; Singh, K.; Upadhyay, S.K. OSCA Genes in Bread Wheat: Molecular Characterization, Expression Profiling, and Interaction Analyses Indicated Their Diverse Roles during Development and Stress Response. *Int. J. Mol. Sci.* **2022**, *23*, 14867. [CrossRef]
22. Kumar, S.; Stecher, G.; Li, M.; Knyaz, C.; Tamura, K. MEGA X: Molecular evolutionary genetics analysis across computing platforms. *Mol. Biol. Evol.* **2018**, *35*, 1547. [CrossRef] [PubMed]
23. Hu, B.; Jin, J.; Guo, A.Y.; Zhang, H.; Luo, J.; Gao, G. GSDS 2.0: An upgraded gene feature visualization server. *Bioinformatics* **2015**, *31*, 1296–1297. [CrossRef] [PubMed]
24. Lescot, M.; Déhais, P.; Thijs, G.; Marchal, K.; Moreau, Y.; Van de Peer, Y.; Rouzé, P.; Rombauts, S. PlantCARE, a database of plant cis-acting regulatory elements and a portal to tools for in silico analysis of promoter sequences. *Nucleic Acids Res.* **2002**, *30*, 325–327. [CrossRef]
25. Gasteiger, E.; Hoogland, C.; Gattiker, A.; Wilkins, M.R.; Appel, R.D.; Bairoch, A. Protein identification and analysis tools on the ExPASy server. In *The proteomics Protocols Handbook*; Humana Press: Totowa, NJ, USA, 2005; pp. 571–607.
26. Yu, C.S.; Chen, Y.C.; Lu, C.H.; Hwang, J.K. Prediction of protein subcellular localization. *Proteins Struct. Funct. Bioinform.* **2006**, *64*, 643–651. [CrossRef] [PubMed]
27. Bailey, T.L.; Boden, M.; Buske, F.A.; Frith, M.; Grant, C.E.; Clementi, L.; Ren, J.; Li, W.W.; Noble, W.S. MEME SUITE: Tools for motif discovery and searching. *Nucleic Acids Res.* **2009**, *37*, 202–208. [CrossRef] [PubMed]
28. Hall, T.; Biosciences, I.; Carlsbad, C.J.G.B.B. BioEdit: An important software for molecular biology. *GERF Bull. Biosci.* **2011**, *2*, 60–61.
29. Choulet, F.; Alberti, A.; Theil, S.; Glover, N.; Barbe, V.; Daron, J.; Pingault, L.; Sourdille, P.; Couloux, A.; Paux, E.; et al. Structural and functional partitioning of bread wheat chromosome 3B. *Science* **2014**, *345*, 1249721. [CrossRef]
30. Pingault, L.; Choulet, F.; Alberti, A.; Glover, N.; Wincker, P.; Feuillet, C.; Paux, E. Deep transcriptome sequencing provides new insights into the structural and functional organization of the wheat genome. *Genome Biol.* **2015**, *16*, 29. [CrossRef]
31. Haas, B.J.; Papanicolaou, A.; Yassour, M.; Grabherr, M.; Blood, P.D.; Bowden, J.; Couger, M.B.; Eccles, D.; Li, B.; Lieber, M.; et al. De novo transcript sequence reconstruction from RNA-seq using the Trinity platform for reference generation and analysis. *Nat. Protoc.* **2013**, *8*, 1494–1512. [CrossRef]
32. Papatheodorou, I.; Fonseca, N.A.; Keays, M.; Tang, Y.A.; Barrera, E.; Bazant, W.; Burke, M.; Füllgrabe, A.; Fuentes, A.M.P.; George, N.; et al. Expression Atlas: Gene and protein expression across multiple studies and organisms. *Nucleic Acids Res.* **2018**, *46*, D246–D251. [CrossRef] [PubMed]
33. Liu, Z.; Xin, M.; Qin, J.; Peng, H.; Ni, Z.; Yao, Y.; Sun, Q. Temporal transcriptome profiling reveals expression partitioning of homeologous genes contributing to heat and drought acclimation in wheat (*Triticum aestivum* L.). *BMC Plant Boil.* **2015**, *15*, 1–20. [CrossRef] [PubMed]
34. Zhang, Y.; Liu, Z.; Khan, A.A.; Lin, Q.; Han, Y.; Mu, P.; Liu, Y.; Zhang, H.; Li, L.; Meng, X.; et al. Expression partitioning of homeologs and tandem duplications contribute to salt tolerance in wheat (*Triticum aestivum* L.). *Sci. Rep.* **2016**, *6*, 21476. [CrossRef] [PubMed]
35. Zhang, H.; Yang, Y.; Wang, C.; Liu, M.; Li, H.; Fu, Y.; Wang, Y.; Nie, Y.; Liu, X.; Ji, W. Large-scale transcriptome comparison reveals distinct gene activations in wheat responding to stripe rust and powdery mildew. *BMC Genom.* **2014**, *15*, 898. [CrossRef] [PubMed]

36. Seo, J.; Gordish-Dressman, H.; Hoffman, E.P. An interactive power analysis tool for microarray hypothesis testing and generation. *Bioinformatics* **2006**, *22*, 808–814. [CrossRef]
37. Sharma, A.; Tyagi, S.; Alok, A.; Singh, K.; Upadhyay, S.K. Thaumatin-like protein kinases: Molecular characterization and transcriptional profiling in five cereal crops. *Plant Sci.* **2020**, *290*, 110317. [CrossRef]
38. Livak, K.J.; Schmittgen, T.D. Analysis of relative gene expression data using real-time quantitative PCR and the $2-\Delta\Delta CT$ method. *Methods* **2001**, *25*, 402–408. [CrossRef]
39. Sharma, A.; Sharma, H.; Rajput, R.; Pandey, A.; Upadhyay, S.K. Molecular Characterization Revealed the Role of Thaumatin-Like Proteins of Bread Wheat in Stress Response. *Front. Plant Sci.* **2022**, *12*, 1664-462X. [CrossRef]
40. Franceschini, A.; Szklarczyk, D.; Frankild, S.; Kuhn, M.; Simonovic, M.; Roth, A.; Lin, J.; Minguez, P.; Bork, P.; Von Mering, C.; et al. STRING v9. 1: Protein-protein interaction networks, with increased coverage and integration. *Nucleic Acids Res.* **2012**, *41*, D808–D815. [CrossRef]
41. Dai, X.; Zhuang, Z.; Zhao, P.X. psRNATarget: A plant small RNA target analysis server (2017 release). *Nucleic Acids Res.* **2018**, *46*, W49–W54. [CrossRef]
42. Knight, H. Calcium signaling during abiotic stress in plants. In *International Review of Cytology*; Academic Press: Cambridge, MA, USA, 1999; Volume 195, pp. 269–324.
43. Aldon, D.; Mbengue, M.; Mazars, C.; Galaud, J.P. Calcium signalling in plant biotic interactions. *Int. J. Mol. Sci.* **2018**, *19*, 665. [CrossRef] [PubMed]
44. Frachisse, J.M.; Thomine, S.; Allain, J.M. Calcium and plasma membrane force-gated ion channels behind development. *Curr. Opin. Plant Biol.* **2020**, *53*, 57–64. [CrossRef] [PubMed]
45. Pei, Z.M.; Murata, Y.; Benning, G.; Thomine, S.; Klüsener, B.; Allen, G.J.; Grill, E.; Schroeder, J.I. Calcium channels activated by hydrogen peroxide mediate abscisic acid ssignalling in guard cells. *Nature* **2000**, *406*, 731–734. [CrossRef]
46. Coste, B.; Xiao, B.; Santos, J.S.; Syeda, R.; Grandl, J.; Spencer, K.S.; Kim, S.E.; Schmidt, M.; Mathur, J.; Dubin, A.E.; et al. Piezo proteins are pore-forming subunits of mechanically activated channels. *Nature* **2012**, *483*, 176–181. [CrossRef]
47. Guo, Y.R.; MacKinnon, R. Structure-based membrane dome mechanism for Piezo mechanosensitivity. *Elife* **2017**, *6*, e33660. [CrossRef]
48. Woo, S.H.; Lukacs, V.; de Nooij, J.C.; Zaytseva, D.; Criddle, C.R.; Francisco, A.; Jessell, T.M.; Wilkinson, K.A.; Patapoutian, A. Piezo2 is the principal mechanotransduction channel for proprioception. *Nat. Neurosci.* **2015**, *18*, 1756–1762. [CrossRef]
49. Rakhshandehroo, F.; Takeshita, M.; Squires, J.; Palukaitis, P. The influence of RNA-dependent RNA polymerase 1 on potato virus Y infection and on other antiviral response genes. *Mol. Plant Microbe Interact.* **2009**, *22*, 1312–1318. [CrossRef] [PubMed]
50. Liao, Y.W.; Sun, Z.H.; Zhou, Y.H.; Shi, K.; Li, X.; Zhang, G.Q.; Xia, X.J.; Chen, Z.X.; Yu, J.Q. The role of hydrogen peroxide and nitric oxide in the induction of plant-encoded RNA-dependent RNA polymerase 1 in the basal defense against *Tobacco mosaic* virus. *PLoS ONE* **2013**, *8*, e76090. [CrossRef]
51. Liao, Y.W.; Liu, Y.R.; Liang, J.Y.; Wang, W.P.; Zhou, J.; Xia, X.J.; Zhou, Y.H.; Yu, J.Q.; Shi, K. The relationship between the plant-encoded RNA-dependent RNA polymerase 1 and alternative oxidase in tomato basal defense against *Tobacco mosaic virus*. *Planta* **2015**, *241*, 641–650. [CrossRef]
52. Cao, J.Y.; Xu, Y.P.; Li, W.; Li, S.S.; Rahman, H.; Cai, X.Z. Genome-wide identification of Dicer-like, Argonaute, and RNA-dependent RNA polymerase gene families in *Brassica* species and functional analyses of their Arabidopsis homologs in resistance to *Sclerotinia sclerotiorum*. *Front. Plant Sci.* **2016**, *7*, 1614. [CrossRef]
53. Koiwa, H.; Li, F.; McCully, M.G.; Mendoza, I.; Koizumi, N.; Manabe, Y.; Nakagawa, Y.; Zhu, J.; Rus, A.; Pardo, J.M.; et al. The STT3a subunit isoform of the Arabidopsis oligosaccharyltransferase controls adaptive responses to salt/osmotic stress. *Plant Cell.* **2003**, *15*, 2273–2284. [CrossRef] [PubMed]
54. Kang, J.S.; Frank, J.; Kang, C.H.; Kajiura, H.; Vikram, M.; Ueda, A.; Kim, S.; Bahk, J.D.; Triplett, B.; Fujiyama, K.; et al. Salt tolerance of *Arabidopsis thaliana* requires maturation of N-glycosylated proteins in the Golgi apparatus. *Proc. Natl. Acad. Sci. USA* **2008**, *105*, 5933–5938. [CrossRef] [PubMed]
55. Németh, K.; Salchert, K.; Putnoky, P.; Bhalerao, R.; Koncz-Kálmán, Z.; Stankovic-Stangeland, B.; Bakó, L.; Mathur, J.; Ökrész, L.; Stabel, S.; et al. Pleiotropic control of glucose and hormone responses by PRL1, a nuclear WD protein, in Arabidopsis. *Genes Dev.* **1998**, *12*, 3059–3073. [CrossRef] [PubMed]
56. Baruah, A.; Šimková, K.; Hincha, D.K.; Apel, K.; Laloi, C. Modulation of 1O2-mediated retrograde signaling by the PLEIOTROPIC RESPONSE LOCUS 1 (PRL1) protein, a central integrator of stress and energy signaling. *Plant J.* **2009**, *60*, 22–32. [CrossRef] [PubMed]
57. Flores-Pérez, Ú.; Pérez-Gil, J.; Closa, M.; Wright, L.P.; Botella-Pavía, P.; Phillips, M.A.; Ferrer, A.; Gershenzon, J.; Rodríguez-Concepción, M. Pleiotropic regulatory locus 1 (PRL1) integrates the regulation of sugar responses with isoprenoid metabolism in Arabidopsis. *Mol. Plant.* **2010**, *3*, 101–112. [CrossRef]
58. Sun, M.; Shen, Y.; Li, H.; Yang, J.; Cai, X.; Zheng, G.; Zhu, Y.; Jia, B.; Sun, X. The multiple roles of OsmiR535 in modulating plant height, panicle branching and grain shape. *Plant Sci.* **2019**, *283*, 60–69. [CrossRef]
59. Zhang, L.L.; Huang, Y.Y.; Zheng, Y.P.; Liu, X.X.; Zhou, S.X.; Yang, X.M.; Liu, S.L.; Li, Y.; Li, J.L.; Zhao, S.L.; et al. *Osa-miR*535 targets SQUAMOSA promoter binding protein-like 4 to regulate blast disease resistance in rice. *Plant J.* **2022**, *110*, 166–178. [CrossRef]
60. Li, W.; Cui, X.; Meng, Z.; Huang, X.; Xie, Q.; Wu, H.; Jin, H.; Zhang, D.; Liang, W. Transcriptional regulation of Arabidopsis *MIR168a* and *argonaute1* homeostasis in abscisic acid and abiotic stress responses. *Plant Physiol.* **2012**, *158*, 1279–1292. [CrossRef]

61. Cui, J.; Jiang, N.; Hou, X.; Wu, S.; Zhang, Q.; Meng, J.; Luan, Y. Genome-wide identification of lncRNAs and analysis of ceRNA networks during tomato resistance to *Phytophthora infestans*. *Phytopathology* **2020**, *110*, 456–464. [CrossRef]
62. Hou, X.; Cui, J.; Liu, W.; Jiang, N.; Zhou, X.; Qi, H.; Meng, J.; Luan, Y. LncRNA39026 enhances tomato resistance to *Phytophthora infestans* by decoying miR168a and inducing PR gene expression. *Phytopathology* **2020**, *110*, 873–880. [CrossRef]
63. Wu, J.; Wang, D.; Liu, Y.; Wang, L.; Qiao, X.; Zhang, S. Identification of miRNAs involved in pear fruit development and quality. *BMC Genom.* **2014**, *15*, 953. [CrossRef] [PubMed]